Available online at www.sciencedirect.com
ScienceDirect
Applied Numerical Mathematics 59 (2009) 1029–1042
APPLIED NUMERICAL MATHEMATICS
www.elsevier.com/locate/apnum

A numerical method for the ternary Cahn–Hilliard system with a degenerate mobility

Junseok Kim [a,*], Kyungkeun Kang [b]

[a] *Department of Mathematics, Korea University, Seoul 136-701, Republic of Korea*
[b] *Department of Mathematics, Sungkyunkwan University and Institute of Basic Sciences, Suwon 440-746, Republic of Korea*

Available online 9 May 2008

Abstract

We applied a second-order conservative nonlinear multigrid method for the ternary Cahn–Hilliard system with a concentration dependent degenerate mobility for a model for phase separation in a ternary mixture. First, we used a standard finite difference approximation for spatial discretization and a Crank–Nicolson semi-implicit scheme for the temporal discretization. Then, we solved the resulting discretized equations using an efficient nonlinear multigrid method. We proved stability of the numerical solution for a sufficiently small time step. We demonstrate the second-order accuracy of the numerical scheme. We also show that our numerical solutions of the ternary Cahn–Hilliard system are consistent with the exact solutions of the linear stability analysis results in a linear regime. We demonstrate that the multigrid solver can straightforwardly deal with different boundary conditions such as Neumann, periodic, mixed, and Dirichlet. Finally, we describe numerical experiments highlighting differences of constant mobility and degenerate mobility in one, two, and three spatial dimensions.
© 2008 IMACS. Published by Elsevier B.V. All rights reserved.

Keywords: Ternary Cahn–Hilliard; Nonlinear multigrid; Phase separation; Degenerate mobility

1. Introduction

The purpose of this work is to consider the conservative nonlinear multigrid method for the ternary Cahn–Hilliard (CH) system with a concentration dependent degenerate mobility for a three component mixture, occupying a domain $\Omega \subset \mathbb{R}^d$ $(d = 1, 2, 3)$. When a homogeneous system composed of three components, at high temperature, is rapidly cooled to a uniform temperature below a critical temperature, where it is unstable with respect to concentration fluctuations, spinodal decomposition takes place: the system separates into spatial regions rich in one specie and poor in the other species. The system evolves into an equilibrium state with lower overall free energy [5].

The composition of a ternary mixture (A, B, and C) can be mapped onto an equilateral triangle (the Gibbs triangle [18]) whose corners represent 100% concentrations of A, B, or C as shown in Fig. 1(a). Mixtures with components lying on lines parallel to $\overline{BC}$ contain the same percentage of A; those with lines parallel to $\overline{AC}$ have the same per-

* Corresponding author.
E-mail addresses: cfdkim@korea.ac.kr (J. Kim), kkang@skku.edu (K. Kang).
URL: http://math.korea.ac.kr/~cfdkim (J. Kim).

0168-9274/$30.00 © 2008 IMACS. Published by Elsevier B.V. All rights reserved.
doi:10.1016/j.apnum.2008.04.004

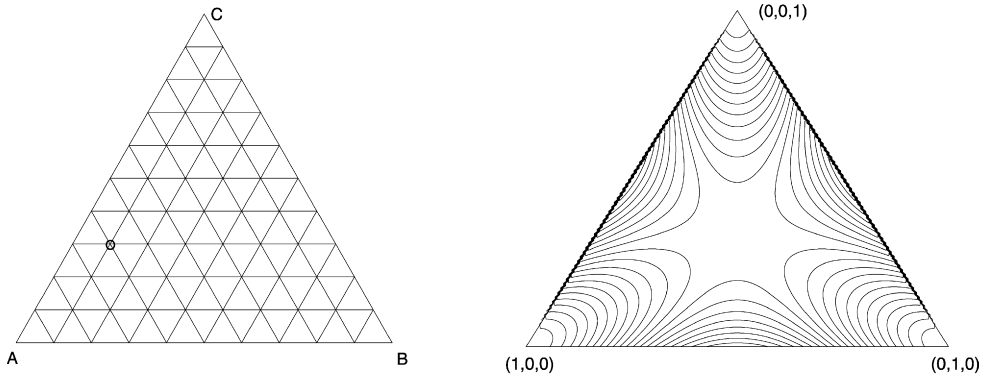

Fig. 1. (a) Gibbs triangle. (b) Contour plot of the free energy $F(\mathbf{c})$.

centage of B concentration; and analogously for the C concentration. In Fig. 1(a), the mixture at the position marked '$\circ$' contains 60% A, 10% B, and 30% C (the total percentage must sum to 100%).

Let $c_i(\mathbf{x}, t)$, $i = 1$, 2, and 3, denote the fractional concentration of the ith component at space $\mathbf{x} \in \Omega$ and time t. We only solve equations for c_1 and c_2 since $c_1 + c_2 + c_3 = 1$, i.e., $\mathbf{c} = (c_1, c_2)$. We define vector gradient, divergence, and Laplace operations as

$$\nabla \mathbf{c} = (\nabla c_1, \nabla c_2), \quad \nabla \cdot \nabla \mathbf{c} = (\nabla \cdot \nabla c_1, \nabla \cdot \nabla c_2), \quad \text{and} \quad \Delta \mathbf{c} = \nabla \cdot \nabla \mathbf{c}.$$

We shall consider the numerical approximation of $\mathbf{c}(\mathbf{x}, t)$ and $\boldsymbol{\mu}(\mathbf{x}, t)$ by solving a system of fourth-order nonlinear diffusion equations given by

$$\frac{\partial \mathbf{c}(\mathbf{x}, t)}{\partial t} = \nabla \cdot \big(M(\mathbf{c}) \nabla \boldsymbol{\mu}(\mathbf{x}, t)\big), \quad \text{for } (\mathbf{x}, t) \in \Omega \times (0, T), \tag{1}$$

$$\boldsymbol{\mu}(\mathbf{x}, t) = \mathbf{f}\big(\mathbf{c}(\mathbf{x}, t)\big) - \Delta \mathbf{c}(\mathbf{x}, t) \boldsymbol{\Gamma}_\epsilon, \tag{2}$$

where

$$M(\mathbf{c}) = \sum_{i<j}^{3} c_i c_j \quad \text{and} \quad \mathbf{f}(\mathbf{c}) = \frac{\partial F(\mathbf{c})}{\partial \mathbf{c}} \equiv \left(\frac{\partial F(\mathbf{c})}{\partial c_1}, \frac{\partial F(\mathbf{c})}{\partial c_2} \right)$$

with the initial condition $\mathbf{c}(\mathbf{x}, 0) = \mathbf{c}^0(\mathbf{x})$. Here $M(\mathbf{c})$ is a concentration dependent mobility, $\boldsymbol{\mu}$ is a generalized chemical potential and $F(\mathbf{c})$ is the free energy of the system. We assume $F(\mathbf{c}) = [c_1^2 c_2^2 + (c_1^2 + c_2^2)(1 - c_1 - c_2)^2]/4$ throughout this paper. Fig. 1(b) shows a contour plot of this free energy, and

$$\boldsymbol{\Gamma}_\epsilon = \begin{pmatrix} 2\epsilon^2 & \epsilon^2 \\ \epsilon^2 & 2\epsilon^2 \end{pmatrix}, \quad \text{where } \epsilon \text{ is a small positive parameter.}$$

The natural and mass conserving boundary conditions for the ternary CH system are the zero Neumann boundary conditions:

$$\nabla \mathbf{c} \cdot \mathbf{n} = \nabla \boldsymbol{\mu} \cdot \mathbf{n} = \mathbf{0} \quad \text{on } \partial\Omega, \tag{3}$$

where $\mathbf{n}$ is the unit normal vector to $\partial\Omega$. Two important aspects of the ternary CH problem in the case of zero Neumann boundary conditions are the conservation of the average $\frac{1}{|\Omega|} \int_\Omega \mathbf{c}(\mathbf{x}, t)\, d\mathbf{x}$ and the existence of a Lyapunov function $\mathcal{E}(\mathbf{c})$,

$$\mathcal{E}(\mathbf{c}) = \int_\Omega \left[F(\mathbf{c}) + \sum_{i=1}^{3} \frac{\epsilon^2}{2} |\nabla c_i|^2 \right] d\mathbf{x}, \tag{4}$$

so that

$$\frac{d}{dt}\mathcal{E}(\mathbf{c}) = -\int_{\Omega} M(\mathbf{c})|\nabla \boldsymbol{\mu}|^2 \, d\mathbf{x}.$$

In this paper, we consider a ternary CH system that we solve by using a second-order accurate conservative finite difference nonlinear multigrid method. The resulting discretization of the ternary CH system (1) and (2)

(i) preserves the mass (average of $\mathbf{c}$) on the discrete level;
(ii) has a discrete equivalent for the Lyapunov functional;
(iii) has a second-order convergence.

Mathematical issues related to the CH equation have been reviewed by Elliott [6]. A generalization of the CH equations to multi-component systems is in Morral and Cahn [17]. Elliott and Luckhaus [10] give a global existence result under constant mobility and with certain assumptions. Eyre [11] discussed differences between multicomponent and binary alloys.

Although there are many numerical works (see [2,6,7,9,8,13,14,12,19] and references therein) with a binary CH equation, much less work has been carried out involving the ternary CH system [4,5,11,16]. But such a system is of considerable practical interest because most engineering alloys consist of more than two components. In [15], a finite difference method is used for the constant mobility. In [3], a finite element approximation is used for the ternary CH system with a degenerate mobility matrix. Multigrid methods are generally accepted as among *the fastest numerical methods* for solving this type of partial differential equations [20]. We use a nonlinear multigrid method to solve resulting equations accurately and efficiently.

The contents of this paper are organized as follows. In Section 2, we consider a fully discrete semi-implicit finite difference scheme and obtain sufficient stability estimates. Also, we describe a nonlinear multigrid V-cycle algorithm for the ternary CH system. Numerical experiments such as a second-order convergence test, comparison with linear stability analysis, different boundary conditions, and effects of a concentration dependent mobility are presented in Section 3. Finally, in Section 4 we conclude.

2. Numerical analysis

In the following numerical scheme and analysis, we restrict space dimensions to two for simplicity. The three-dimensional extension is straightforward.

2.1. Discretization

Let $\Omega = [a, b] \times [c, d] \subset \mathbb{R}^2$ be partitioned by

$$a = x_{\frac{1}{2}} < x_{1+\frac{1}{2}} < \cdots < x_{N_x-1+\frac{1}{2}} < x_{N_x+\frac{1}{2}} = b,$$
$$c = y_{\frac{1}{2}} < y_{1+\frac{1}{2}} < \cdots < y_{N_x-1+\frac{1}{2}} < y_{N_y+\frac{1}{2}} = d.$$

For simplicity, we assume the above partitions are uniform in both directions and the grid size is h. We denote by $\Omega_h = \{(x_i, y_j)\colon 1 \leqslant i \leqslant N_x, 1 \leqslant j \leqslant N_y\}$ set of cell centered points $(x_i, y_j) = ((x_{i-\frac{1}{2}} + x_{i+\frac{1}{2}})/2, (y_{j-\frac{1}{2}} + y_{j+\frac{1}{2}})/2)$.

Let $\mathbf{c}_{ij}$ and $\boldsymbol{\mu}_{ij}$ be approximations of $\mathbf{c}(x_i, y_j)$ and $\boldsymbol{\mu}(x_i, y_j)$. We first implement the zero Neumann boundary condition (3) by requiring that

$$D_x\mathbf{c}_{\frac{1}{2},j} = D_x\mathbf{c}_{N_x+\frac{1}{2},j} = D_y\mathbf{c}_{i,\frac{1}{2}} = D_y\mathbf{c}_{i,N_y+\frac{1}{2}} = \mathbf{0},$$
$$D_x\boldsymbol{\mu}_{\frac{1}{2},j} = D_x\boldsymbol{\mu}_{N_x+\frac{1}{2},j} = D_y\boldsymbol{\mu}_{i,\frac{1}{2}} = D_y\boldsymbol{\mu}_{i,N_y+\frac{1}{2}} = \mathbf{0},$$

where the discrete differentiation operators are

$$D_x\mathbf{c}_{i+\frac{1}{2},j} = (\mathbf{c}_{i+1,j} - \mathbf{c}_{ij})/h \quad \text{and} \quad D_y\mathbf{c}_{i,j+\frac{1}{2}} = (\mathbf{c}_{i,j+1} - \mathbf{c}_{ij})/h.$$

We then define the discrete Laplacian by

$$\Delta_h\mathbf{c}_{ij} = (D_x\mathbf{c}_{i+\frac{1}{2},j} - D_x\mathbf{c}_{i-\frac{1}{2},j} + D_y\mathbf{c}_{i,j+\frac{1}{2}} - D_y\mathbf{c}_{i,j-\frac{1}{2}})/h$$

and the discrete l^2 inner product by

$$(\mathbf{c}, \mathbf{d})_h = h^2 \sum_{i=1}^{N_x} \sum_{j=1}^{N_y} (c_{1ij} d_{1ij} + c_{2ij} d_{2ij}). \tag{5}$$

For a grid function $\mathbf{c}$ defined at the cell centers, $D_x\mathbf{c}$ and $D_y\mathbf{c}$ are defined at the cell-edges. We use the following notation

$$\nabla_h \mathbf{c}_{ij} = (D_x \mathbf{c}_{i+\frac{1}{2},j}, D_y \mathbf{c}_{i,j+\frac{1}{2}}),$$

to represent the discrete gradient of $\mathbf{c}$. We can define an inner product for $\nabla_h\mathbf{c}$ on the staggered grid by

$$\begin{aligned}(\nabla_h \mathbf{c}, \nabla_h \mathbf{d})_h = h^2 \Bigg[&\sum_{i=0}^{N_x} \sum_{j=1}^{N_y} (D_x c_{1 i+\frac{1}{2},j} D_x d_{1 i+\frac{1}{2},j} + D_x c_{2 i+\frac{1}{2},j} D_x d_{2 i+\frac{1}{2},j}) \\ &+ \sum_{i=1}^{N_x} \sum_{j=0}^{N_y} (D_y c_{1 i,j+\frac{1}{2}} D_y d_{1 i,j+\frac{1}{2}} + D_y c_{2 i,j+\frac{1}{2}} D_y d_{2 i,j+\frac{1}{2}}) \Bigg].\end{aligned} \tag{6}$$

We also define discrete norms associated with (5) and (6) as

$$\|\mathbf{c}\|^2 = (\mathbf{c}, \mathbf{c})_h, \qquad |\mathbf{c}|_1^2 = (\nabla_h \mathbf{c}, \nabla_h \mathbf{c})_h.$$

The time-continuous, space-discrete system that corresponds to (1) and (2) is

$$\frac{d}{dt}\mathbf{c}_{ij} = \nabla_h \cdot \big[M(\mathbf{c}_{ij}) \nabla_h \boldsymbol{\mu}_{ij}\big], \quad \boldsymbol{\mu}_{ij} = \mathbf{f}(\mathbf{c}_{ij}) - \Delta_h \mathbf{c}_{ij} \boldsymbol{\Gamma}_\epsilon, \tag{7}$$

where the boundary conditions are implemented using (3). The scheme has a discrete energy functional given by the discretization of (4).

We discretize (7) in time by using the Crank–Nicolson algorithm:

$$\frac{\mathbf{c}_{ij}^{n+1} - \mathbf{c}_{ij}^n}{\Delta t} = \nabla_h \cdot \big[M(\mathbf{c}_{ij})_{ij}^{n+\frac{1}{2}} \nabla_h \boldsymbol{\mu}_{ij}^{n+\frac{1}{2}}\big], \tag{8}$$

$$\boldsymbol{\mu}_{ij}^{n+\frac{1}{2}} = \frac{1}{2}\big(\mathbf{f}(\mathbf{c}_{ij}^{n+1}) + \mathbf{f}(\mathbf{c}_{ij}^n)\big) - \frac{1}{2}\Delta_h(\mathbf{c}_{ij}^{n+1} + \mathbf{c}_{ij}^n)\boldsymbol{\Gamma}_\epsilon, \tag{9}$$

where $\boldsymbol{\mu}_{ij}^{n+\frac{1}{2}} = (\boldsymbol{\mu}_{ij}^{n+1} + \boldsymbol{\mu}_{ij}^n)/2$.

2.2. Stability

In this subsection, assuming that the nonlinear system at an implicit time step is solvable, we establish the mass conservation and demonstrate that the energy functional is nonincreasing in time provided that the step size of time is sufficiently small. We show the mass conservation and energy dissipation in the next theorem.

Theorem 1. *Let* $\{\mathbf{c}^{n+1}, \boldsymbol{\mu}^{n+1}\}$ *be the solution of* (8) *and* (9)*, and the discrete energy functional be given by*

$$\mathcal{E}(\mathbf{c}^n) = \big(F(\mathbf{c}^n), 1\big)_h + \frac{\epsilon^2}{2}\|\nabla_h \mathbf{c}^n\|_m^2, \tag{10}$$

where

$$\begin{aligned}\|\nabla_h \mathbf{c}^n\|_m^2 &:= |c_1^n|_1^2 + |c_2^n|_1^2 + |1 - c_1^n - c_2^n|_1^2 \\ &= 2|c_1^n|_1^2 + 2|c_2^n|_1^2 + 2(\nabla_h c_1^n, \nabla_h c_2^n).\end{aligned}$$

Suppose that the numerical solution $\mathbf{c}^n$ *is bounded. Then*

$$(\mathbf{c}^{n+1}, 1)_h = (\mathbf{c}^n, 1)_h, \tag{11}$$

and there exists an absolute constant C depending only on Ω such that

$$\mathcal{E}(\mathbf{c}^{n+1}) - \mathcal{E}(\mathbf{c}^n) \leqslant -\mathcal{R}_h \Delta t \big(M(\mathbf{c})^{n+\frac{1}{2}} \nabla_h \boldsymbol{\mu}^{n+\frac{1}{2}}, \nabla_h \boldsymbol{\mu}^{n+\frac{1}{2}}\big)_h, \tag{12}$$

where

$$\mathcal{R}_h = \left(1 - \frac{C\|D^2 F(\cdot)\|_{L^\infty}\|M(\cdot)\|_{L^\infty}\Delta t}{h^2}\right).$$

Moreover, $\mathcal{E}(\mathbf{c}^{n+1}) \leqslant \mathcal{E}(\mathbf{c}^n)$ for all n provided that Δt is sufficiently small.

Proof. The mass conservation is straightforward by using summation by parts. Indeed,

$$(\mathbf{c}^{n+1}, 1)_h = \big(\mathbf{c}^n + \Delta t \nabla_h \cdot \big[M(\mathbf{c})^{n+\frac{1}{2}} \nabla_h \boldsymbol{\mu}^{n+\frac{1}{2}}\big], 1\big)_h = (\mathbf{c}^n, 1)_h.$$

First, by multiplying (8) and (9) by $\boldsymbol{\mu}^{n+\frac{1}{2}}$ and $\mathbf{c}^{n+1} - \mathbf{c}^n$, we obtain the following two identities:

$$(\mathbf{c}^{n+1} - \mathbf{c}^n, \boldsymbol{\mu}^{n+\frac{1}{2}})_h + \Delta t \big(M(\mathbf{c})^{n+\frac{1}{2}} \nabla_h \boldsymbol{\mu}^{n+\frac{1}{2}}, \nabla_h \boldsymbol{\mu}^{n+\frac{1}{2}}\big)_h = 0 \tag{13}$$

and

$$(\boldsymbol{\mu}^{n+\frac{1}{2}}, \mathbf{c}^{n+1} - \mathbf{c}^n)_h = \frac{1}{2}\big(\mathbf{f}(\mathbf{c}^{n+1}) + \mathbf{f}(\mathbf{c}^n), \quad \mathbf{c}^{n+1} - \mathbf{c}^n\big)_h + \frac{\epsilon^2}{2}\big(|\mathbf{c}^{n+1}|_m^2 - |\mathbf{c}^n|_m^2\big). \tag{14}$$

Since the first identity (13) is straightforward, the details are omitted. Thus we need to verify only the second one (14). Indeed,

$$\begin{aligned}(\boldsymbol{\mu}^{n+\frac{1}{2}}, \mathbf{c}^{n+1} - \mathbf{c}^n)_h &= \frac{1}{2}\big(\mathbf{f}(\mathbf{c}^{n+1}) + \mathbf{f}(\mathbf{c}^n) - \boldsymbol{\Gamma}_\epsilon \Delta_h(\mathbf{c}^{n+1} + \mathbf{c}^n), \mathbf{c}^{n+1} - \mathbf{c}^n\big)_h \\ &= \frac{1}{2}\big(\mathbf{f}(\mathbf{c}^{n+1}) + \mathbf{f}(\mathbf{c}^n), \quad \mathbf{c}^{n+1} - \mathbf{c}^n\big)_h - \frac{1}{2}\big(\boldsymbol{\Gamma}_\epsilon \Delta_h(\mathbf{c}^{n+1} + \mathbf{c}^n)\boldsymbol{\Gamma}_\epsilon, \mathbf{c}^{n+1} - \mathbf{c}^n\big)_h.\end{aligned}$$

The second term on the right side is calculated:

$$\begin{aligned}\big(\boldsymbol{\Gamma}_\epsilon(\Delta\mathbf{c}^{n+1} + \Delta\mathbf{c}^n), \mathbf{c}^{n+1} - \mathbf{c}^n\big) &= \begin{pmatrix} 2\epsilon^2 & \epsilon^2 \\ \epsilon^2 & 2\epsilon^2 \end{pmatrix}\begin{pmatrix} \Delta c_1^{n+1} + \Delta c_1^n \\ \Delta c_2^{n+1} + \Delta c_2^n \end{pmatrix} \cdot \begin{pmatrix} c_1^{n+1} - c_1^n \\ c_2^{n+1} - c_2^n \end{pmatrix} \\ &= -2\epsilon^2\big(|\mathbf{c}^{n+1}|_1^2 - |\mathbf{c}^n|_1^2\big) - 2\epsilon^2(\nabla_h c_2^{n+1}, \nabla_h c_1^{n+1}) + 2\epsilon^2(\nabla_h c_2^n, \nabla_h c_1^n) \\ &= -2\epsilon^2\big(|\mathbf{c}^{n+1}|_1^2 + (\nabla_h c_2^{n+1}, \nabla_h c_1^{n+1})\big) + 2\epsilon^2\big(|\mathbf{c}^n|_1^2 + (\nabla_h c_2^n, \nabla_h c_1^n)\big) \\ &= -\epsilon^2\|\nabla_h \mathbf{c}^{n+1}\|_m^2 + \epsilon^2\|\nabla_h \mathbf{c}^n\|_m^2.\end{aligned}$$

This completes the derivation of (14). Next, using our scheme (8) and (9), we also have the following estimates.

$$\|\mathbf{c}^{n+1} - \mathbf{c}^n\|^2 \leqslant \frac{C\Delta t^2}{h^2}\big\|M(\mathbf{c})^{n+\frac{1}{2}} \nabla_h \boldsymbol{\mu}^{n+\frac{1}{2}}\big\|^2, \tag{15}$$

$$|\mathbf{c}^{n+1} - \mathbf{c}^n|_1^2 \leqslant \frac{C\Delta t^2}{h^4}\big\|M(\mathbf{c})^{n+\frac{1}{2}} \nabla_h \boldsymbol{\mu}^{n+\frac{1}{2}}\big\|^2, \tag{16}$$

where C depends on Ω. To show (15), multiplying $\mathbf{c}^{n+1} - \mathbf{c}^n$ to (8),

$$\|\mathbf{c}^{n+1} - \mathbf{c}^n\|^2 = \Delta t\big(M(\mathbf{c})^{n+\frac{1}{2}} \nabla_h \boldsymbol{\mu}^{n+\frac{1}{2}}, \nabla_h(\mathbf{c}^{n+1} - \mathbf{c}^n)\big).$$

On the other hand, we can easily check the following inequality:

$$|\mathbf{c}^{n+1} - \mathbf{c}^n|_1^2 \leqslant \frac{C}{h^2}\|\mathbf{c}^{n+1} - \mathbf{c}^n\|^2.$$

Combining the above inequalities, we get

$$\|\mathbf{c}^{n+1} - \mathbf{c}^n\| \leqslant \frac{C\Delta t}{h}\big\|M(\mathbf{c})^{n+\frac{1}{2}} \nabla_h \boldsymbol{\mu}^{n+\frac{1}{2}}\big\|,$$

where we used a discrete Hölder inequality. The estimate (16) is an easy consequence of the estimate (15). Indeed,

$$|\mathbf{c}^{n+1}-\mathbf{c}^n|_1^2 \leqslant \frac{C}{h^2}\|\mathbf{c}^{n+1}-\mathbf{c}^n\|^2 \leqslant \frac{C\Delta t^2}{h^4}\big\|M(\mathbf{c})^{n+\frac{1}{2}}\nabla_h\boldsymbol{\mu}^{n+\frac{1}{2}}\big\|^2.$$

Now we consider

$$\begin{aligned}\mathcal{E}(\mathbf{c}^{n+1})-\mathcal{E}(\mathbf{c}^n) &= \big(F(\mathbf{c}^{n+1})-F(\mathbf{c}^n),1\big)_h + \frac{\epsilon^2}{2}\big(|\mathbf{c}^{n+1}|_m^2-|\mathbf{c}^n|_m^2\big)\\ &= \big(F(\mathbf{c}^{n+1})-F(\mathbf{c}^n),1\big)_h + (\boldsymbol{\mu}^{n+\frac{1}{2}},\mathbf{c}^{n+1}-\mathbf{c}^n)_h - \frac{1}{2}\big(\mathbf{f}(\mathbf{c}^{n+1})+\mathbf{f}(\mathbf{c}^n),\mathbf{c}^{n+1}-\mathbf{c}^n\big)_h\\ &= \big(F(\mathbf{c}^{n+1})-F(\mathbf{c}^n),1\big)_h - \frac{1}{2}\big(\mathbf{f}(\mathbf{c}^{n+1})+\mathbf{f}(\mathbf{c}^n),\mathbf{c}^{n+1}-\mathbf{c}^n\big)_h\\ &\quad -\Delta t\big(M(\mathbf{c})^{n+\frac{1}{2}}\nabla_h\boldsymbol{\mu}^{n+\frac{1}{2}},\nabla_h\boldsymbol{\mu}^{n+\frac{1}{2}}\big)_h,\end{aligned}$$

where we used the identities (13) and (14). Since F is differentiable, we have

$$\begin{aligned}\big(F(\mathbf{c}^{n+1})-F(\mathbf{c}^n),1\big)_h &= \left(\int_0^1 \frac{d}{d\theta}F\big(\theta\mathbf{c}^{n+1}+(1-\theta)\mathbf{c}^n\big)\,d\theta,1\right)_h\\ &= \left(\int_0^1 \frac{\partial}{\partial\mathbf{c}}F\big(\theta\mathbf{c}^{n+1}+(1-\theta)\mathbf{c}^n\big)\,d\theta,\mathbf{c}^{n+1}-\mathbf{c}^n\right)_h.\end{aligned}$$

Therefore, using the identity above, we have

$$\begin{aligned}&\big(F(\mathbf{c}^{n+1})-F(\mathbf{c}^n),1\big)_h - \frac{1}{2}\big(\mathbf{f}(\mathbf{c}^{n+1})+\mathbf{f}(\mathbf{c}^n),\mathbf{c}^{n+1}-\mathbf{c}^n\big)_h\\ &= \left(\int_0^1\left[\frac{\partial}{\partial\mathbf{c}}F\big(\theta\mathbf{c}^{n+1}+(1-\theta)\mathbf{c}^n\big)-\frac{1}{2}\left(\frac{\partial}{\partial\mathbf{c}}F(\mathbf{c}^{n+1})+\frac{\partial}{\partial\mathbf{c}}F(\mathbf{c}^n)\right)\right]d\theta,\ \mathbf{c}^{n+1}-\mathbf{c}^n\right)_h\\ &\leqslant \|D^2F\|_{L^\infty}\|\mathbf{c}^{n+1}-\mathbf{c}^n\|^2 \leqslant \frac{C\|D^2F\|_{L^\infty}\Delta t^2}{h^2}\big\|M(\mathbf{c})^{n+\frac{1}{2}}\nabla_h\boldsymbol{\mu}^{n+\frac{1}{2}}\big\|^2,\end{aligned}$$

where D^2F indicates the Hessian of F and we used the estimate (15). Since F is smooth and the numeric solution $\mathbf{c}^k$ is assumed to be uniformly bounded for all k, it is obvious that $\|D^2F\|_{L^\infty}$ is also uniformly bounded.

Here we note that, due to the nonnegativity of $M(\mathbf{c})$, we observe the following estimate:

$$\big\|M(\mathbf{c})^{n+\frac{1}{2}}\nabla_h\boldsymbol{\mu}^{n+\frac{1}{2}}\big\|^2 \leqslant \big\|M(\cdot)\big\|_{L^\infty}\big(M(\mathbf{c})^{n+\frac{1}{2}}\nabla_h\boldsymbol{\mu}^{n+\frac{1}{2}},\nabla_h\boldsymbol{\mu}^{n+\frac{1}{2}}\big).$$

In the above estimate we again used that $M(\cdot)$ is smooth and the numeric solution $\mathbf{c}^k$ is bounded for all k. Summing the above estimates, we obtain

$$\begin{aligned}\mathcal{E}(\mathbf{c}^{n+1})-\mathcal{E}(\mathbf{c}^n) &\leqslant -\Delta t\big(M(\mathbf{c})^{n+\frac{1}{2}}\nabla_h\boldsymbol{\mu}^{n+\frac{1}{2}},\nabla_h\boldsymbol{\mu}^{n+\frac{1}{2}}\big)_h + \|D^2F\|_{L^\infty}\|\mathbf{c}^{n+1}-\mathbf{c}^n\|^2\\ &\leqslant -\Delta t\big(M(\mathbf{c})^{n+\frac{1}{2}}\nabla_h\boldsymbol{\mu}^{n+\frac{1}{2}},\nabla_h\boldsymbol{\mu}^{n+\frac{1}{2}}\big)_h\\ &\quad + \frac{C\|D^2F(\cdot)\|_{L^\infty}\|M(\cdot)\|_{L^\infty}\Delta t^2}{h^2}\big(M(\mathbf{c})^{n+\frac{1}{2}}\nabla_h\boldsymbol{\mu}^{n+\frac{1}{2}},\nabla_h\boldsymbol{\mu}^{n+\frac{1}{2}}\big)_h\\ &= -\Delta t\big(M(\mathbf{c})^{n+\frac{1}{2}}\nabla_h\boldsymbol{\mu}^{n+\frac{1}{2}},\nabla_h\boldsymbol{\mu}^{n+\frac{1}{2}}\big)_h\left(1-\frac{C\|D^2F(\cdot)\|_{L^\infty}\|M(\cdot)\|_{L^\infty}\Delta t}{h^2}\right).\end{aligned}$$

Therefore, if Δt is taken to be sufficiently small, then the discrete energy is dissipated. More precisely, if we choose Δt:

$$\Delta t \leqslant \frac{h^2}{C\|D^2F(\cdot)\|_{L^\infty}\|M(\cdot)\|_{L^\infty}},$$

then we have $\mathcal{E}(\mathbf{c}^{n+1}) \leqslant \mathcal{E}(\mathbf{c}^n)$ for all n. This completes the proof. □

Table 1
l_2 convergence result

32–64	rate	64–128	rate	128–256	rate	256–512
6.8629e − 2	2.3335	1.3616e − 2	2.1575	3.0521e − 3	2.1450	6.9008e − 4

2.3. A nonlinear multigrid V-cycle algorithm

In this section, we describe a nonlinear Full Approximation Storage (FAS) multigrid method to solve the nonlinear discrete system at the implicit time level. The nonlinearity, $\mathbf{f}(\mathbf{c})$, is treated using one step of Newton's iteration. A pointwise Gauss–Seidel relaxation scheme is used as the smoother in the multigrid method. One *SMOOTH* relaxation operator step consists of solving the system (17) and (18) given below by 4×4 matrix inversion for each ij. First, let us discretize Eq. (8).

$$\begin{aligned}&\frac{\bar{\mathbf{c}}_{ij}^m}{\Delta t} + \frac{M_{i+\frac{1}{2},j} + M_{i-\frac{1}{2},j} + M_{i,j+\frac{1}{2}} + M_{i,j-\frac{1}{2}}}{h^2}\bar{\boldsymbol{\mu}}_{ij}^{m-\frac{1}{2}}\\ &\quad = \boldsymbol{\phi}_{ij}^n + \frac{M_{i+\frac{1}{2},j}\boldsymbol{\mu}_{i+1,j}^{m-\frac{1}{2}} + M_{i-\frac{1}{2},j}\bar{\boldsymbol{\mu}}_{i-1,j}^{m-\frac{1}{2}} + M_{i,j+\frac{1}{2}}\boldsymbol{\mu}_{i,j+1}^{m-\frac{1}{2}} + M_{i,j-\frac{1}{2}}\bar{\boldsymbol{\mu}}_{i,j-1}^{m-\frac{1}{2}}}{h^2},\end{aligned} \tag{17}$$

where $M_{i+\frac{1}{2},j} = M((\mathbf{c}_{ij}^m + \mathbf{c}_{i+1,j}^m + \mathbf{c}_{ij}^n + \mathbf{c}_{i+1,j}^n)/4)$ and the other terms are similarly defined. Next, let us discretize Eq. (9). Since $\mathbf{f}(\mathbf{c}_{ij}^{n+1})$ is nonlinear with respect to $\mathbf{c}_{ij}^{n+1}$, we linearize $\mathbf{f}(\mathbf{c}_{ij}^{n+1})$ at $\mathbf{c}_{ij}^m$, i.e.,

$$\begin{aligned}&\mathbf{f}(\mathbf{c}_{ij}^{n+1}) \approx \mathbf{f}(\mathbf{c}_{ij}^m) + (\bar{\mathbf{c}}_{ij}^m - \mathbf{c}_{ij}^m)\frac{\partial \mathbf{f}(\mathbf{c}_{ij}^m)}{\partial \mathbf{c}},\\ &-\bar{\mathbf{c}}_{ij}^m\left(\frac{\partial \mathbf{f}(\mathbf{c}_{ij}^m)}{2\partial \mathbf{c}} + \frac{2}{h^2}\boldsymbol{\Gamma}_\epsilon\right) + \bar{\boldsymbol{\mu}}_{ij}^{m-\frac{1}{2}} = \boldsymbol{\psi}_{ij}^n + \frac{1}{2}\mathbf{f}(\mathbf{c}_{ij}^m) - \mathbf{c}_{ij}^m\frac{\partial \mathbf{f}(\mathbf{c}_{ij}^m)}{2\partial \mathbf{c}}\\ &\qquad\qquad - \frac{1}{2h^2}(\mathbf{c}_{i+1,j}^m + \bar{\mathbf{c}}_{i-1,j}^m + \mathbf{c}_{i,j+1}^m + \bar{\mathbf{c}}_{i,j-1}^m)\boldsymbol{\Gamma}_\epsilon.\end{aligned} \tag{18}$$

See the reference text [20] for additional details.

3. Numerical experiments

In this section, we perform a convergence test, linear stability analysis, and comparisons between constant and degenerate mobilities.

3.1. Convergence test

To obtain an estimate of the rate of convergence, we perform a number of simulations for a sample initial problem on a set of increasingly finer grids. The initial condition is

$$\begin{aligned}&c_1(x) = 0.25 + 0.01\cos(3\pi x) + 0.04\cos(5\pi x),\\ &c_2(x) = 0.25 - 0.02\cos(2\pi x) + 0.01\cos(4\pi x)\end{aligned} \tag{19}$$

on a domain, $\Omega = [0, 1]$. The numerical solutions are computed on the uniform grids, $h = 1/2^n$ and with corresponding time steps, $\Delta t = 0.1h$ for $n = 5$, 6, 7, 8, and 9. The calculations are run up to time $T = 0.2$ and $\epsilon = 0.005$ is used.

We define the error to be the discrete l_2-norm of the difference between that grid and the average of the next finer grid cells covering it: $\mathbf{e}_{h/\frac{h}{2}i} := \mathbf{c}_{hi} - (\mathbf{c}_{\frac{h}{2}2i} + \mathbf{c}_{\frac{h}{2}2i-1})/2$. The rate of convergence is defined as: $\log_2(\|\mathbf{e}_{h/\frac{h}{2}}\|/\|\mathbf{e}_{\frac{h}{2}/\frac{h}{4}}\|)$.

The errors and rates of convergence are given in Table 1. The results suggest that the scheme is indeed second order accurate.

In Fig. 2, the time evolution of the total energy (10) with the same initial data (19) is shown. Also, the inscribed small figures are the concentration fields (c_1: solid, c_2: dotted, and $1 - c_1 - c_2$: dashed lines) at the indicated times. As expected from Theorem 1, the total energy is nonincreasing and tends to a constant value.

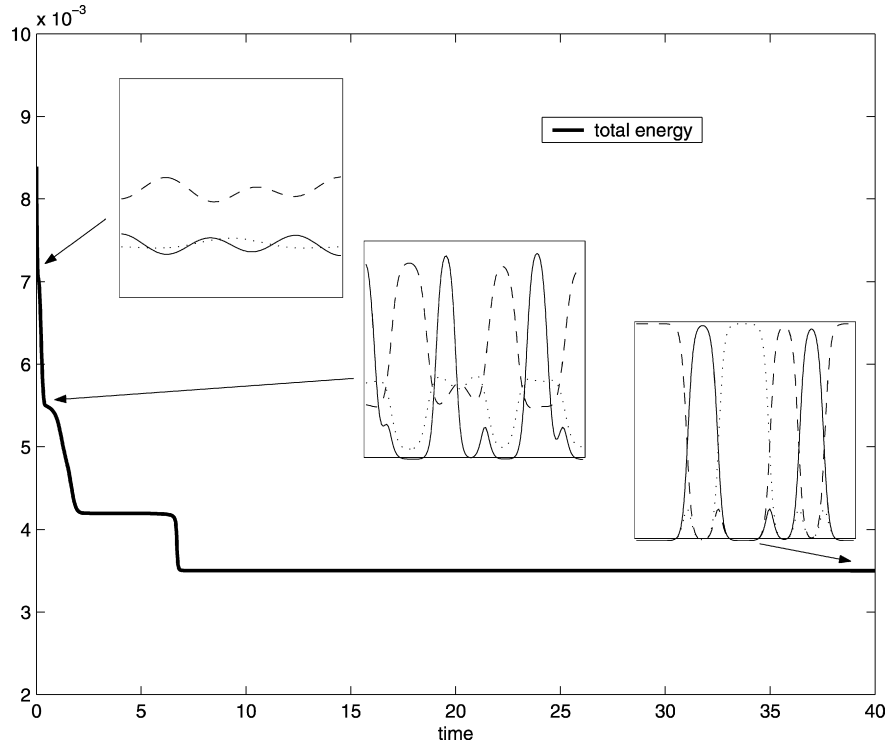

Fig. 2. The time evolution of the total energy (10) of the numerical solutions with the initial data (19). Snapshots of the concentration fields (c_1: solid, c_2: dotted, and $1 - c_1 - c_2$: dashed lines) are shown.

3.2. Linear stability analysis

To fix ideas, we consider a ternary system in the one dimensional domain, $\Omega = [0, 1]$ and $M(\mathbf{c}) \equiv 1$. The partial differential equations (1) and (2) we wish to solve may be written as

$$\frac{\partial \mathbf{c}(x,t)}{\partial t} = \Delta\left(\frac{\partial F(\mathbf{c})}{\partial \mathbf{c}} - \Delta \mathbf{c}\boldsymbol{\Gamma}_\epsilon\right), \quad \text{where } (x,t) \in \Omega \times (0,T]. \tag{20}$$

Let the mean concentration take the form $\mathbf{m} = (m_1, m_2)$. We seek a solution of the form

$$\mathbf{c}(x,t) = \mathbf{m} + \sum_{k=1}^{\infty} \cos(k\pi x)\big(\alpha_k(t), \beta_k(t)\big), \quad \text{where } \big|\alpha_k(t)\big|, \big|\beta_k(t)\big| \ll 1.$$

After linearizing $\partial F(\mathbf{c})/\partial \mathbf{c}$ about $\mathbf{m}$, we have

$$\frac{\partial F(\mathbf{c})}{\partial \mathbf{c}} \approx \frac{\partial F(\mathbf{m})}{\partial \mathbf{c}} + (\mathbf{c} - \mathbf{m}) \begin{pmatrix} \partial_c^2 F(\mathbf{m}) & \partial_c \partial_d F(\mathbf{m}) \\ \partial_c \partial_d F(\mathbf{m}) & \partial_d^2 F(\mathbf{m}) \end{pmatrix}. \tag{21}$$

Substituting (21) into (20) and letting $m_1 = m_2 = m$ for simplicity, then, up to first order, we have

$$\frac{\partial \mathbf{c}}{\partial t} = \Delta \mathbf{c} \begin{pmatrix} 7.5m^2 - 4m + 0.5 & 6m^2 - 2m \\ 6m^2 - 2m & 7.5m^2 - 4m + 0.5 \end{pmatrix} - \Delta^2 \mathbf{c}\boldsymbol{\Gamma}_\epsilon. \tag{22}$$

After substituting $\mathbf{c} = \mathbf{m} + \cos(k\pi x)(\alpha_k(t), \beta_k(t))$ into (22), we obtain

$$\begin{pmatrix} \alpha_k(t) \\ \beta_k(t) \end{pmatrix}' = \mathbf{A} \begin{pmatrix} \alpha_k(t) \\ \beta_k(t) \end{pmatrix}, \quad \mathbf{A} = \begin{pmatrix} a & b \\ b & a \end{pmatrix}, \tag{23}$$

where $'$ is time derivative and

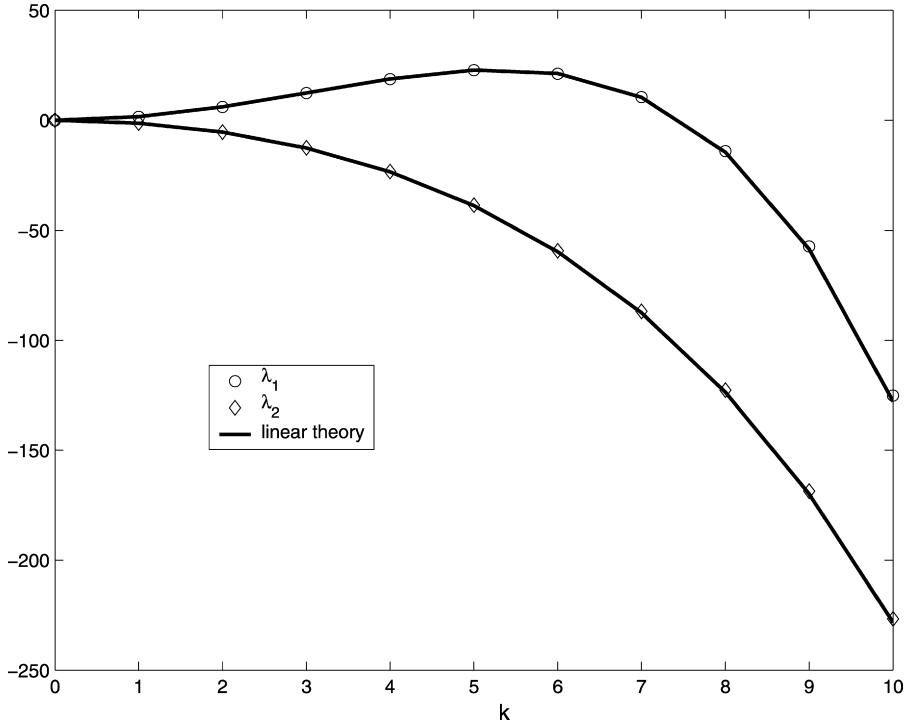

Fig. 3. Growth rates for the different wave number k.

$$a = -(k\pi)^2\big[7.5m^2 - 4m + 0.5 + 2\epsilon^2(k\pi)^2\big],$$
$$b = -(k\pi)^2\big[6m^2 - 2m + \epsilon^2(k\pi)^2\big].$$

The solution to the system of *ODE*s (23) is given by

$$\begin{pmatrix}\alpha_k(t)\\ \beta_k(t)\end{pmatrix} = e^{\mathbf{A}t}\begin{pmatrix}\alpha_k(0)\\ \beta_k(0)\end{pmatrix}.$$

The eigenvalues of $\mathbf{A}$ are

$$\lambda_1 = -(k\pi)^2\big[13.5m^2 - 6m + 0.5 + 3\epsilon^2(k\pi)^2\big], \tag{24}$$
$$\lambda_2 = -(k\pi)^2\big[1.5m^2 - 2m + 0.5 + \epsilon^2(k\pi)^2\big]. \tag{25}$$

In Fig. 3, the theoretical growth rates λ_1 and λ_2 are compared to those obtained from the nonlinear numerical scheme. The numerical growth rate is defined by

$$\tilde{\lambda} = \log\left(\frac{\max_j |c_i(x_j, T) - 0.22|}{\max_j |c_i(x_j, 0) - 0.22|}\right)\Big/T, \quad i = 1, 2.$$

Here, we used $m = 0.22$, $\epsilon = 0.01$, $\Delta t = 10^{-3}$, $h = 1/128$, and $T = 0.02$. In Fig. 3, the symbol '$\circ$' is a numerical result, which is compared with the theoretical values λ_1 (solid line) with initial condition $c_1(x) = c_2(x) = 0.22 + 0.001\cos(k\pi x)$. The symbol '$\diamond$' is a numerical result, which is compared with λ_2 (solid line) with initial conditions $c_1(x) = 0.22 + 0.001\cos(k\pi x)$ and $c_2(x) = 0.22 - 0.001\cos(k\pi x)$.

3.3. Comparisons between different boundary conditions

In this section, we demonstrate the capabilities of the multigrid solver in the ternary Cahn–Hilliard equation with different boundary conditions such as Neumann, periodic, mixed, and Dirichlet. The initial condition is

$$c_1(x, y) = 1/3 + 0.01\,\mathrm{rand}(x, y), \qquad c_2(x, y) = 1/3 + 0.01\,\mathrm{rand}(x, y),$$

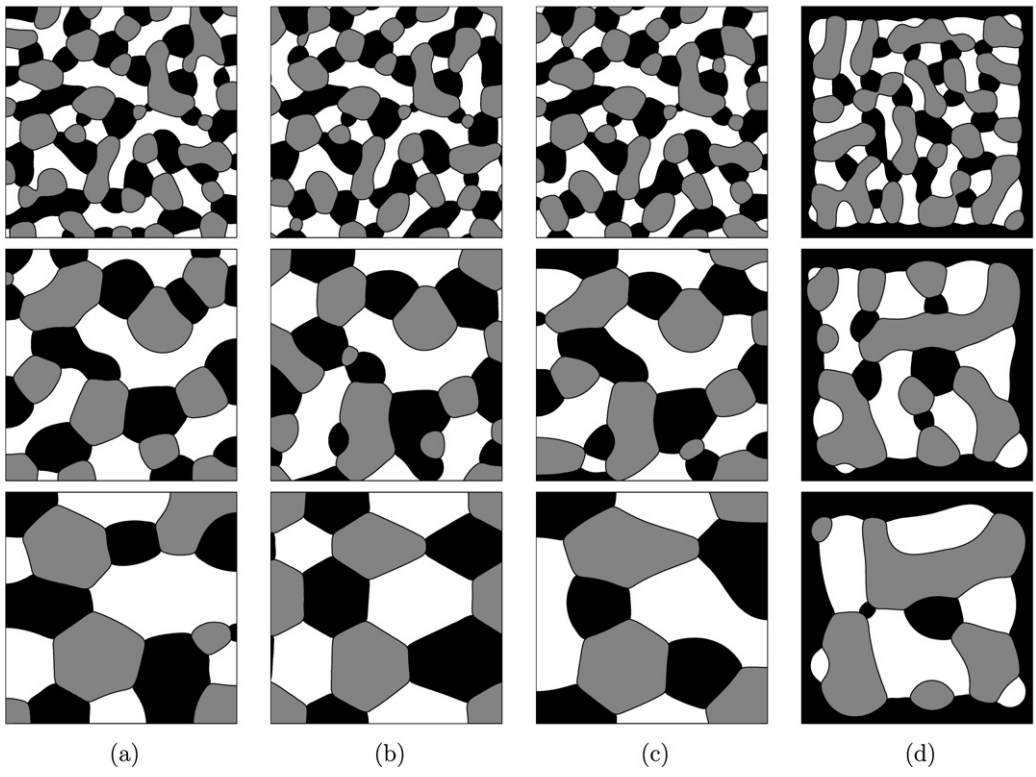

Fig. 4. (a) Neumann boundary; (b) Periodic boundary; (c) Mixed boundary (Neumann in x direction and periodic in y direction); (d) Dirichlet ($c_2(x,0) = c_2(x,1) = c_2(0,y) = c_2(1,y) = 1$) boundary. Times are $t = 0.1$, 0.68, and 3.91 (from top to bottom).

where the random number, rand(x, y), is in $[-1, 1]$ and has zero mean. A 128×128 mesh is used on the unit square $\Omega = [0,1] \times [0,1]$ and we choose $h = 1/128$, $\Delta t = 0.1h$, and $\epsilon = 0.004$. In Fig. 4, the medium, darkest, and lightest shades of gray represent the first, second and third components of mixture, respectively. From the first column to the fourth column are Neumann, periodic, mixed (Neumann in x direction and periodic in y direction), and Dirichlet ($c_2(x,0) = c_2(x,1) = c_2(0,y) = c_2(1,y) = 1$) boundary conditions, respectively. The temporal evolution is from top to bottom. As each column shows, the multigrid method can straightforwardly deal with various boundary conditions.

3.4. Comparisons between constant and degenerate mobilities

In this section, we demonstrate the fundamental difference between a degenerate and a constant mobility using the proposed numerical method. The reduction of the total amount of interfacial area is the main driving force in the CH system both for degenerate and for constant mobility. In the case of degenerate mobility this is done only by local adjustment in connected phase regions, whereas in the case of constant mobility also nonlocal interactions are used to achieve this. In the case of a constant mobility, diffusion through bulk regions is still possible and disconnected regions influence each other in order to decrease the total amount of interfacial area. For long times, constant CH systems generally lead to situations where each phase occupies only one connected part of the domain [1].

3.4.1. One space dimension

We perform a degenerate and a constant mobility experiment with an initial condition,

$$c_1(x) = 1/3 + 0.1\,\text{rand}(x), \qquad c_2(x) = 1/3 + 0.1\,\text{rand}(x).$$

A 128 grid is used on the interval $\Omega = [0,1]$. We choose $h = 1/128$, $\Delta t = 0.1h$, and $\epsilon = 0.01$. We consider that the numerical computations reach a numerical equilibrium state when the discrete l_2-norm of the difference between $(n+1)$th- and nth-time steps becomes less than 10^{-7}, i.e., $\|\mathbf{c}^{n+1} - \mathbf{c}^n\| \leqslant 10^{-7}$.

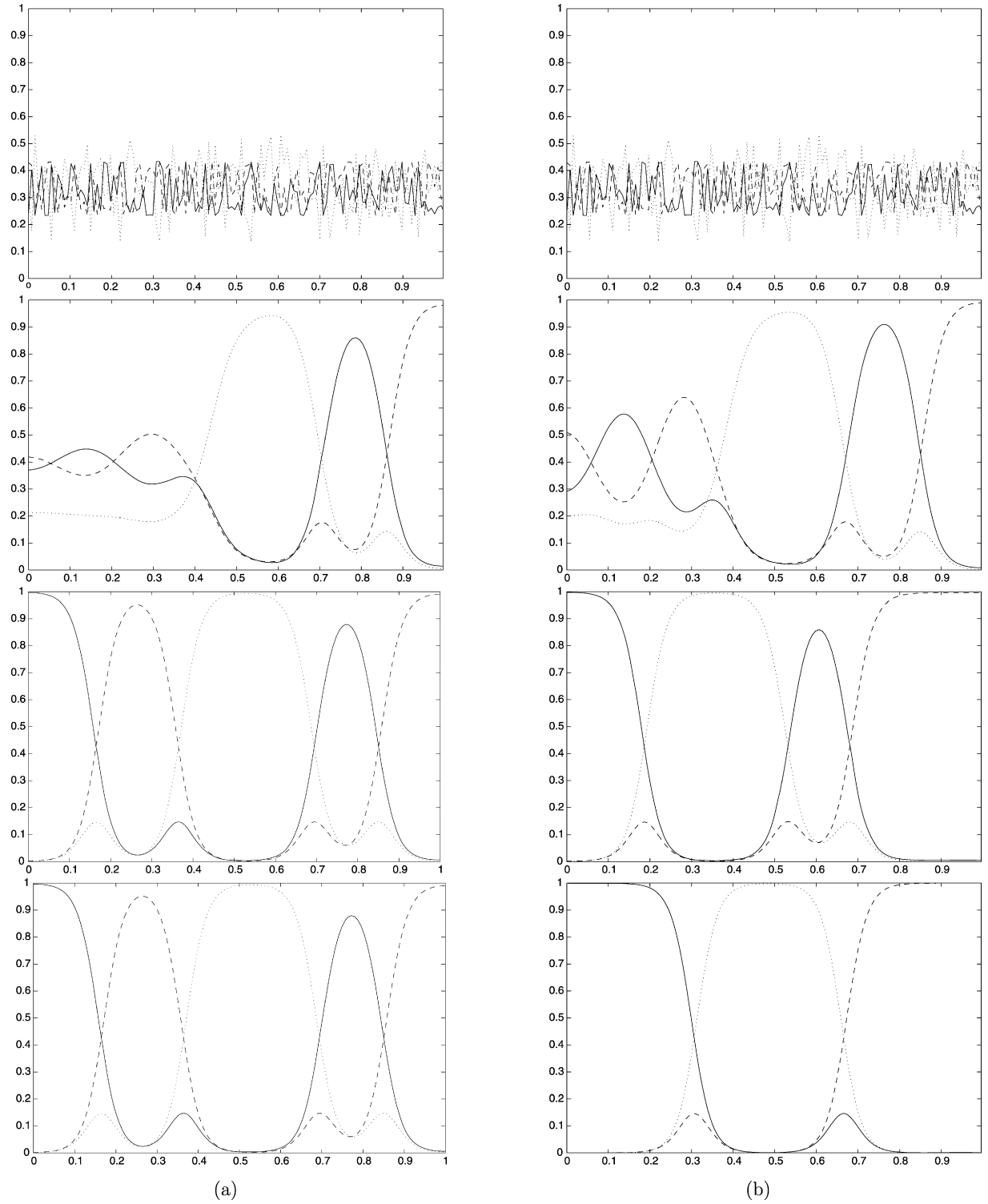

Fig. 5. Long time evolution of a ternary system with $(m_1, m_2, m_3) = (\frac{1}{3}, \frac{1}{3}, \frac{1}{3})$. Columns (a) and (b) show the evolution of a degenerate and a constant mobility system, respectively, at time $t = 0.0$, 5.5, 62.5, and 70.3 (from top to bottom). Solid, dotted, and dashed lines are c_1, c_2, and $1 - c_1 - c_2$, respectively.

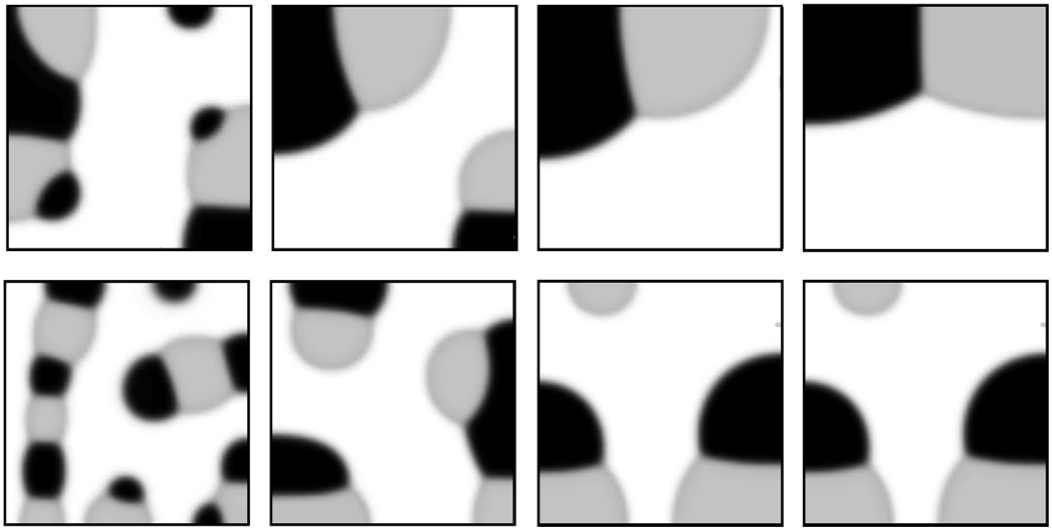

Fig. 6. The top and the bottom row is the evolution of constant and degenerate mobility, respectively. The times are $t = 9.77$, 68.36, 195.31, and 380.86 (from left to right).

The pictures in Fig. 5 are arranged with time increasing from the top to the bottom ($t = 0.0$, 5.5, 62.5, and 70.3). Column (a) is a degenerate mobility and column (b) is a constant mobility. The final numerical solutions plotted in Fig. 5 are stationary numerical solutions.

3.4.2. Two space dimensions

We now perform a degenerate and a constant mobility numerical experiment with the initial data,

$$c_1(x, y) = 0.22 + 0.1\,\mathrm{rand}(x, y), \qquad c_2(x, y) = 0.22 + 0.1\,\mathrm{rand}(x, y).$$

A 64×64 mesh is used on the unit square $\Omega = [0, 1] \times [0, 1]$ and we choose $h = 1/64$, $\Delta t = 0.1h$, and $\epsilon = 0.004$.

In Fig. 6, the medium, darkest, and lightest shades of gray represent the first, second and third components of mixture, respectively. The first row is a constant mobility and the second row is a degenerate mobility. We note that the final pictures of each row in Fig. 6 show numerical stationary solutions of a constant and a degenerate mobility, respectively.

3.4.3. Three space dimensions

The following example illustrates our method's potential for modeling phase separation in three spatial dimensions. We now perform a degenerate and a constant mobility numerical experiment with the initial data,

$$c_1(x, y, z) = 0.22 + 0.1\,\mathrm{rand}(x, y, z), \qquad c_2(x, y, z) = 0.22 + 0.1\,\mathrm{rand}(x, y, z).$$

A $32 \times 32 \times 32$ mesh is used on the unit cube $\Omega = [0, 1] \times [0, 1] \times [0, 1]$. We choose $h = 1/32$, $\Delta t = 0.2h$, and $\epsilon = 0.01$.

We illustrate the evolution of this initial condition in Fig. 7. In Fig. 7, the medium, darkest and lightest shades of gray represent the first, second and third components of the mixture, respectively. The first row is a constant mobility and the second row is a degenerate mobility. We note that the final pictures of each row in Fig. 7 show numerical stationary solutions of a constant and a degenerate mobility, respectively.

4. Conclusions

We considered a fully discrete semi-implicit finite difference scheme for the ternary CH system with a degenerate mobility. We solved the resulting scheme by an efficient nonlinear multigrid method and obtained sufficient stability estimates. We carried out numerical experiments such as a second-order convergence test, comparison with linear stability analysis, the multigrid treatment on different boundary conditions, and phase separation in the ternary system

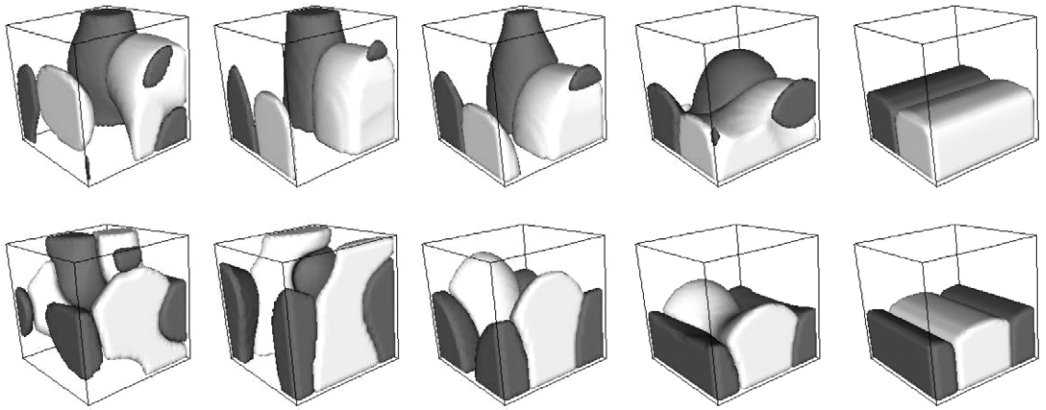

Fig. 7. The top row (times are $t = 12.5$, 25.0, 50.0, 62.5, and 75.0) and the bottom row (the times are $t = 12.5$, 50.0, 212.5, 250.0, and 312.5) is the evolution of constant and degenerate mobility, respectively.

with a constant and a degenerate mobility. We found, in the case of a constant mobility, the diffusion through bulk regions is still possible and that disconnected regions influence each other, leading to situations where each phase occupies only one connected part of the domain after long times. Whereas, in the case of a degenerate mobility, we found each phase could occupy disconnected parts of the domain.

Acknowledgements

This research was supported by the MKE (Ministry of Knowledge Economy), Korea, under the ITRC (Information Technology Research Center) support program supervised by the IITA (Institute for Information Technology Advancement) (IITA-2008-C1090-0801-0013). This work was also supported by the Korea Research Foundation Grant funded by the Korean Government (MOEHRD) (KRF-2006-C00225). The second author was supported partially by KRF-2006-331-C00020.

References

[1] J.W. Barrett, J.F. Blowey, Finite element approximation of a model for phase separation of a multi-component alloy with non-smooth free energy, Numer. Math. 77 (1997) 1–34.
[2] J.W. Barrett, J.F. Blowey, Finite element approximation of the Cahn–Hilliard equation with concentration dependent mobility, Math. Comp. 68 (1999) 487–517.
[3] J.W. Barrett, J.F. Blowey, H. Garcke, On fully practical finite element approximations of degenerate Cahn–Hilliard systems, M2AN Math. Model. Numer. Anal. 35 (2001) 713–748.
[4] J.F. Blowey, M.I.M. Copetti, C.M. Elliott, Numerical analysis of a model for phase separation of a multi-component alloy, IMA J. Numer. Anal. 16 (1996) 111–139.
[5] M.I.M. Copetti, Numerical experiments of phase separation in ternary mixtures, Math. Comput. Simulation 52 (2000) 41–51.
[6] C.M. Elliott, The Cahn–Hilliard model for the kinetics of phase separation, in: J.F. Rodrigues (Ed.), Mathematical Models for Phase Change Problems, Birkhäuser Verlag, Basel, 1989.
[7] C.M. Elliott, D.A. French, A nonconforming finite-element method for the two-dimensional Cahn–Hilliard equation, SIAM J. Numer. Anal. 26 (1989) 884–903.
[8] C.M. Elliott, D. French, F. Milner, A second order splitting method for the Cahn–Hilliard equation, Numer. Math. 54 (1989) 575–590.
[9] C.M. Elliott, S. Larsson, Error estimates with smooth and nonsmooth data for a finite element method for the Cahn–Hilliard equation, Math. Comp. 58 (1992) 603–630.
[10] C.M. Elliott, S. Luckhaus, A generalized diffusion equation for phase separation of a multicomponent mixture with interfacial free energy, IMA, University of Minnesota, Preprint, 887, 1991.
[11] D.J. Eyre, Systems of Cahn–Hilliard equations, SIAM J. Appl. Math. 53 (1993) 1686–1712.
[12] D.A. French, J.W. Schaeffer, Continuous finite element methods which preserve energy properties for nonlinear problems, Appl. Math. Comput. 39 (1990) 271–295.
[13] D. Furihata, Finite difference schemes for $\frac{\partial u}{\partial t} = (\frac{\partial}{\partial x})^{\alpha} \frac{\delta G}{\delta u}$ that inherit energy conservation or dissipation property, J. Comput. Phys. 156 (1999) 181–205.
[14] D. Furihata, A stable and conservative finite difference scheme for the Cahn–Hilliard equation, Numer. Math. 87 (2001) 675–699.
[15] J.S. Kim, K. Kang, J.S. Lowengrub, Conservative multigrid methods for ternary Cahn–Hilliard systems, Comm. Math. Sci. 2 (2004) 53–77.

[16] S. Maier-Paape, B. Stoth, T. Wanner, Spinodal decomposition for multicomponent Cahn–Hilliard systems, J. Statist. Phys. 98 (2000) 871–896.
[17] J.E. Morral, J.W. Cahn, Spinodal decomposition in ternary system, Acta Metall. 19 (1971) 1037–1045.
[18] D.A. Porter, K.E. Easterling, Phase Transformations in Metals and Alloys, Chapman and Hall, London, 1992.
[19] Z.Z. Sun, A second-order accurate linearized difference scheme for the two-dimensional Cahn–Hilliard equation, Math. Comp. 64 (1995) 1463–1471.
[20] U. Trottenberg, C. Oosterlee, A. Schüller, Multigrid, Academic Press, San Diego, CA, 2001.